Continuous Exposure-Time Modeling for Realistic Atmospheric Turbulence Synthesis

CVPR26

背景

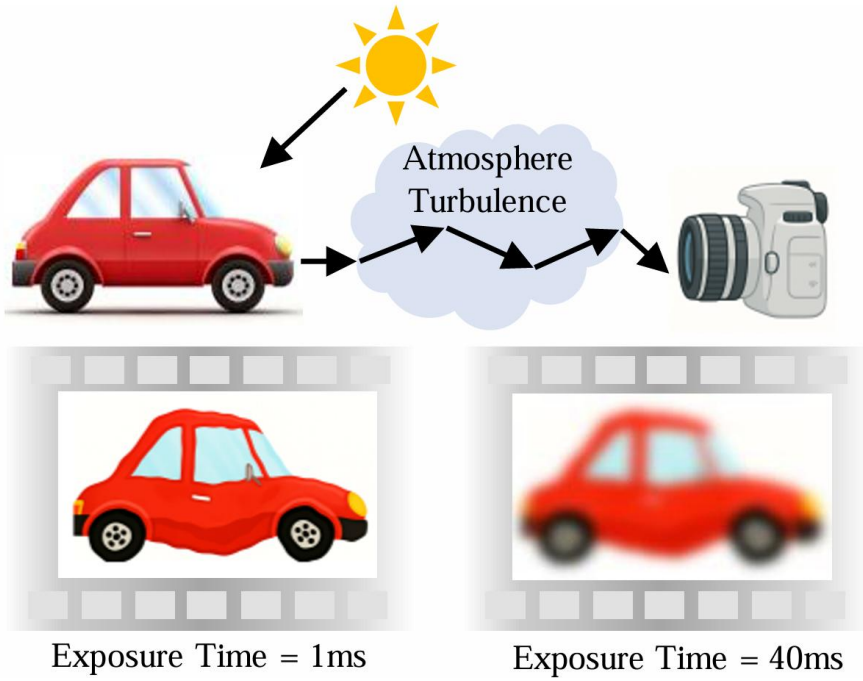

Figure 1. Imaging results under atmospheric turbulence with different exposure-time. **Short-exposure** (e.g., 1 ms) primarily exhibits turbulence-induced **tilt** due to effectively frozen instantaneous turbulence states. In contrast, **long-exposure** (e.g., 40 ms) integrates multiple turbulent states over time, resulting in significantly stronger **blur**.

- 当光线穿过大气层传播并被成像系统接收时,**大气湍流**会导致获得的图像出现严重**退化**,主要表现为图像模糊和倾斜变形等现象，不仅破坏了图像的视觉质量,更严重影响后续图像处理和分析的效果。

- 对于相机而言，曝光时间的大小会决定相机捕获的图像的清晰度:
  短曝光时间： 在短曝光时间下（1 ms），可以近似视作瞬间的湍流状态被冻结在相机中，使得湍流对于图像的影响以扭曲为主。
- **长曝光时间**： 在长曝光时间下（40 ms），相机在一个较长的时间窗口内持续接收光线，这使得大气中的湍流对图像的影响累积，使得湍流对于图像的影响以模糊为主。

大气湍流建模

大气湍流模型

湍流退化图像的形成可以用数学模型来模拟：

$$I(\mathbf{x}) = \mathcal{H}(J(\mathbf{x})) = \mathcal{B}(\mathcal{T}(J(\mathbf{x})))$$

其中，$J(\mathbf{x})$表示干净图像，$\mathbf{x}$为空间像素位置，$H(\cdot)$表示整体湍流退化操作，可以分解为两个操作，即：**扭曲操作** $T(\cdot)$和**模糊操作** $B(\cdot)$，$I(\mathbf{x})$为最终湍流退化图像。

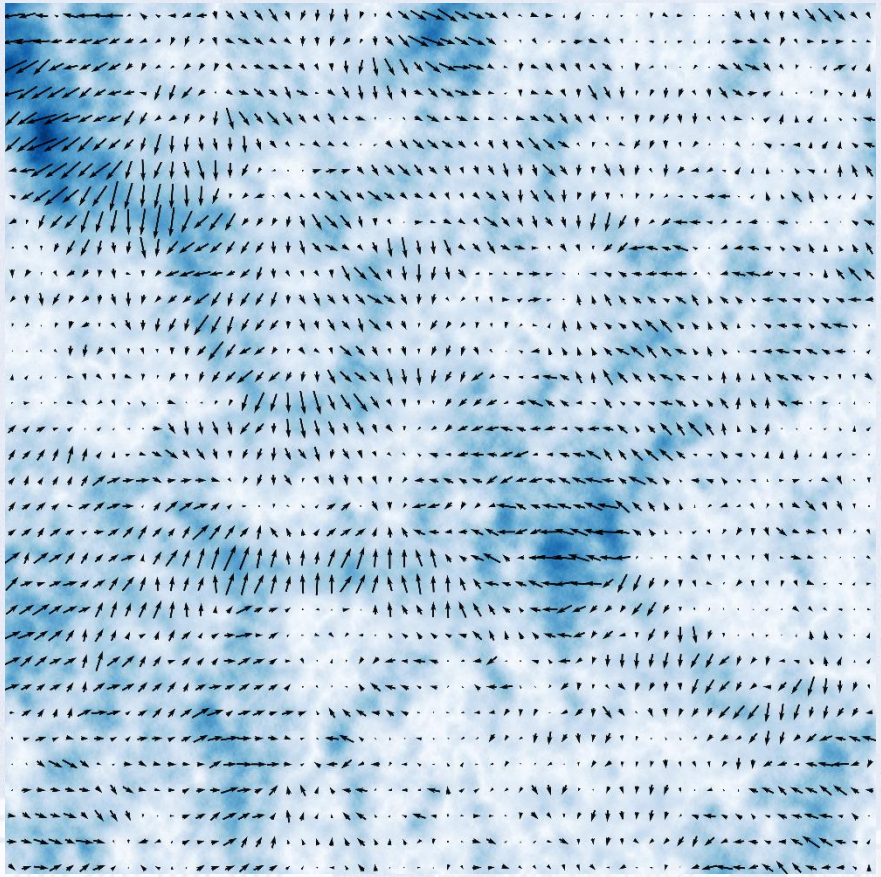

扭曲操作

对于扭曲部分，我们直接引用Schwartzman的建模方法[1]，将扭曲退化设置为像素点的二维移动，通过空间相关的**二维位移场**来表示扭曲。

[1] Schwartzman A, Alterman M, Zamir R, et al. Turbulence-induced 2d correlated image distortion[C]//2017 IEEE international conference on computational photography (ICCP). IEEE, 2017: 1-13.

大气湍流建模

模糊操作

湍流引起的模糊在数学上被描述为卷积操作：

$$\mathcal{B}(I_T(\mathbf{x})) = \mathrm{PSF}(\mathbf{x}) * I_T(\mathbf{x})$$

$I_T(x)$表示倾斜图像，PSF(x)表示点扩散函数，＊表示卷积。在**频域**，PSF可以通过傅里叶变换转化为光学传递函数OTF：

$$\mathrm{OTF}(\boldsymbol{\xi}) = \mathcal{F}\{\mathrm{PSF}(\mathbf{x})\} = \mathrm{MTF}(\boldsymbol{\xi})\, e^{i\cdot \mathrm{PhTF}(\boldsymbol{\xi})}$$

其中MTF(ξ)为编码**模糊**效果的调制传递函数，PhTF(ξ)为编码**倾斜**效果的相位传递函数。ξ表示空间频率，高频对应边缘等精细图像细节，低频代表粗结构和整体场景构成。在我们的任务中，只对纯模糊建模，因此仅仅关注MTF：

$$\mathcal{B}(I_T(\boldsymbol{\xi})) = \mathrm{MTF}(\boldsymbol{\xi}) \cdot I_T(\boldsymbol{\xi})$$

大气湍流建模

大气湍流MTF

目前对于大气湍流MTF的研究主要将其分为两种状态：**长曝光**和**短曝光**。

在**短曝光**状态下，曝光时间足够短可以视作大气湍流保持冻结状态，从而导致传感器记录瞬时湍流实现，图像以倾斜和微弱模糊为主。

$$\mathrm{MTF}_{\mathrm{SE}}(\boldsymbol{\xi}) = e^{-57.4aC_n^2L\lambda^{-1/3}\|\boldsymbol{\xi}\|^{5/3}\left[1-\mu\left(\left(\frac{\lambda\|\boldsymbol{\xi}\|}{D}\right)^{1/3}\right)\right]}$$

式中a表示为球面波时设置为3/8，平面波时设置为1，Cn^2为湍流强度参数，L为传播距离，λ为波长，μ在远场为0.5，近场为1，D为光学孔径。

在**长曝光**状态下，传感器随着时间的推移集成了多个快速变化的湍流状态，导致强模糊的逐渐积累。

$$\mathrm{MTF}_{\mathrm{LE}}(\boldsymbol{\xi}) = e^{-57.4aC_n^2L\lambda^{-1/3}\|\boldsymbol{\xi}\|^{5/3}}$$

曝光时间依赖的模糊算子

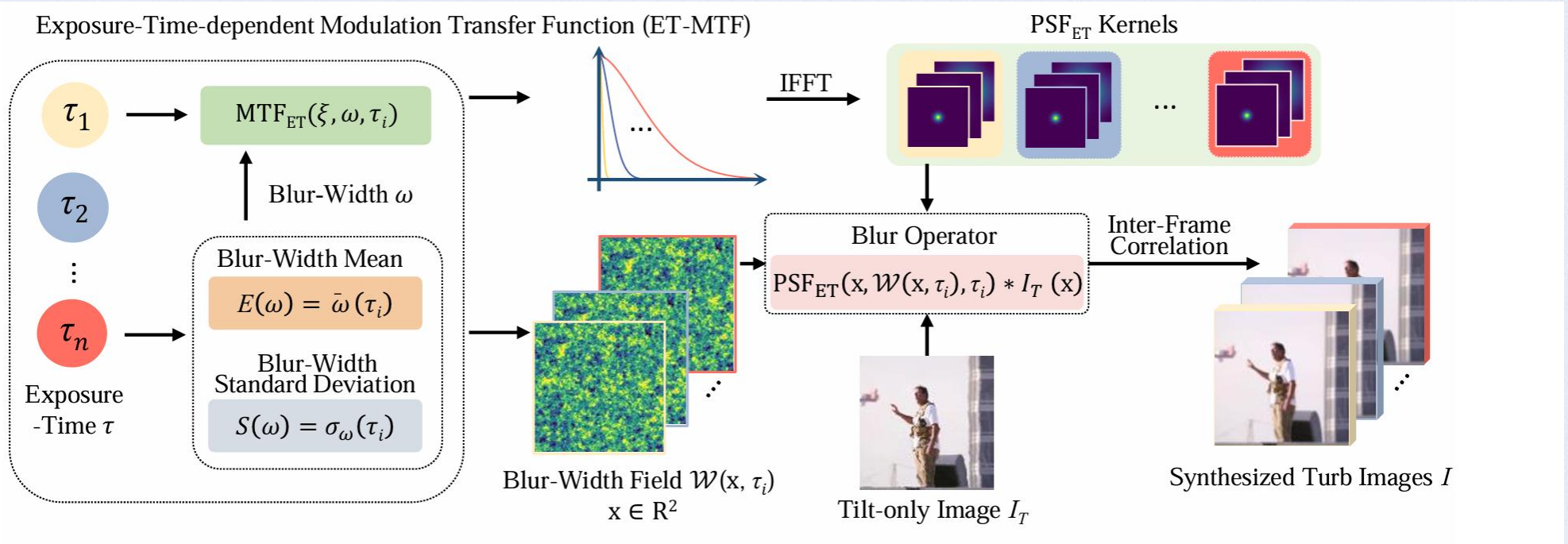

Figure 2. Overview of the proposed exposure-time-dependent turbulence synthesis pipeline. The exposure-time τ is treated as a continuous input parameter to both the ET-MTF and blur-width field formulations. By systematically varying τ, our pipeline generates turbulence-degraded images with physically consistent blur characteristics from the input tilt image.

曝光时间依赖的模糊算子

ET-MTF

为了模拟全曝光时间范围内的模糊退化，我们扩展了Azoulay 最初提出的有限曝光MTF理论[2]。Azoulay假设，在短曝光条件下，传感器捕捉到涡流有效冻结在孔径D的湍流状态。在长曝光条件下，传感器随着时间的推移集成连续的湍流状态，近似地将湍流冻结在更大的有效孔径内。

$$\mathrm{MTF}_{\mathrm{ET}}(\boldsymbol{\xi},\tau) = e^{-\left(\frac{\lambda\|\boldsymbol{\xi}\|}{\rho_p(\tau)}\right)^{5/3}} \qquad \rho_p(\tau) = 1 + 0.35\left(\frac{r_0}{D + v_w\tau}\right)^{1/3}$$

其中r_0为Fried参数，v_w为风速。

然而，大气湍流由于局部折射率波动而表现出空间变化的模糊模式。上述方法仅能生成空间不变的模糊，我们根据模糊宽度重新参数化ET-MTF。模糊宽度ω定义为PSF 的全宽半高（FWHM）的一半：

$$\omega \approx \frac{0.49\lambda f}{r_0}$$

最终得到的ET-MTF可以用下式表示：

$$\mathrm{MTF}_{\mathrm{ET}}(\boldsymbol{\xi},\omega,\tau) = e^{-\left(\frac{\lambda\|\boldsymbol{\xi}\|}{\rho_p(\omega,\tau)}\right)^{5/3}} \qquad \rho_p(\omega,\tau) = 1 + 0.28\left(\frac{\lambda f}{\omega(D + v_w\tau)}\right)^{1/3}$$

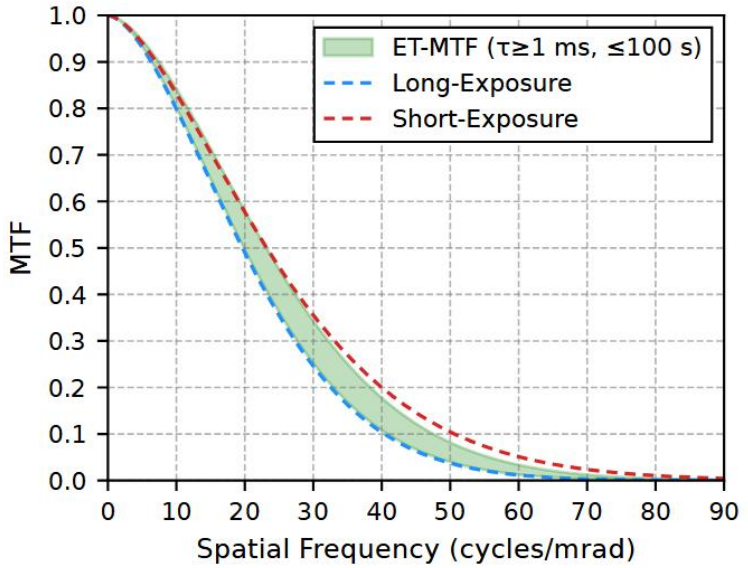

Figure 3. Comparison of MTF formulations at short and long-exposure limits. ET-MTF shows a smooth evolution of the MTF as exposure-time varies between the short and long-exposure limits.

[2] Azoulay E. Effects on Atmospheric Turbulence on the MTF of Imaging Systems[J]. Bericht FGAN-FfO, 1990, 3.

曝光时间依赖的模糊算子

模糊宽度场

为了将PSF公式扩展到整个图像域，我们定义了一个空间变化的**模糊宽度场**W(x,τ)。该字段为每个空间位置分配一个局部模糊尺度，从而实现空间非均匀模糊的建模。

他受到理论均值和标准差的约束[3]：

$$\overline{\omega}(\tau) = \frac{2.44\lambda}{D} \times \left(1 + 0.268\left(\frac{D}{r_0}\right)^{5/3} + \frac{1.792\left(\frac{D}{r_0}\right)^{5/3}}{1 + \left(0.97\frac{D}{v_w \tau}\right)^{0.607}}\right)^{0.5}$$

$$\sigma_\omega(\tau) = 1.70\frac{r_0^{1/3}}{\lambda}\left(DC_n^2 L\right)^{0.5} \times \left(1 - \frac{1}{1 + \left(4.45\frac{D}{v_w \tau}\right)^{0.5}}\right)^{0.5}$$

最终模糊算子可以用以下公式表达：

$$\mathcal{B}_\tau(I_T(\mathbf{x})) = \mathrm{PSF}_{\mathrm{ET}}(\mathbf{x},\ \mathcal{W}(\mathbf{x},\tau),\ \tau) * I_T(\mathbf{x})$$

[3] Du Bosq T W, Repasi E. Detector integration time dependent atmospheric turbulence imaging simulation[C]//Infrared Imaging Systems: Design, Analysis, Modeling, and Testing XXVI. SPIE, 2015, 9452: 101-113.

曝光时间依赖的模糊算子

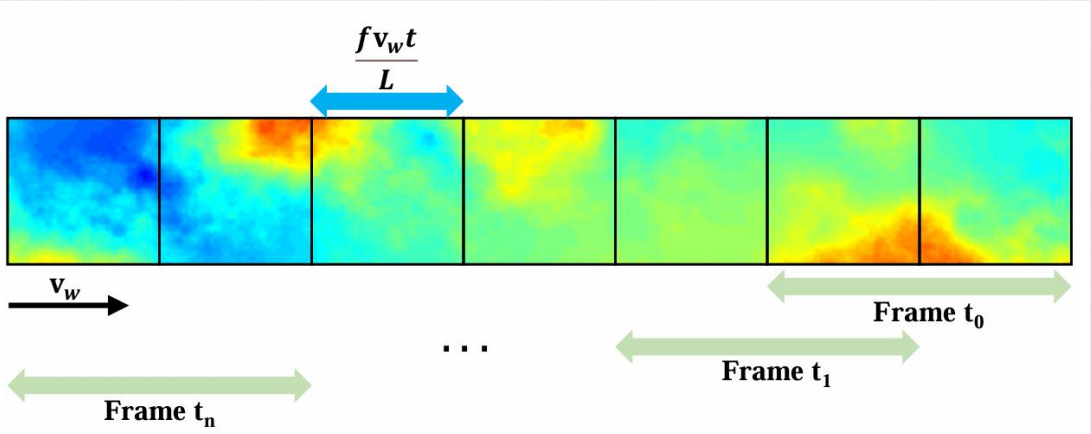

Figure 4. Temporal evolution of turbulence degradation under Taylor's frozen-flow hypothesis in video synthesis. We construct an extended turbulence degradation field along the wind direction $\mathbf{v}_w$. Temporal correlation between frames is achieved by displacing this field over time using the shift $\frac{f\mathbf{v}_w t}{L}$.

帧间相关性

将湍流合成从单个图像扩展到视频序列需要建模大气退化如何在连续帧之间演变。我们采用Taylor的冻结流假设，该假设将湍流视为冻结状态，沿着风向进行平移。因此，视频帧间的退化过程可以建模为冻结退化场的空间平移：

$$\mathcal{H}(J_t(\mathbf{x})) = \mathcal{H}\left(J_0\left(\mathbf{x} - \frac{f\mathbf{v}_w t}{L}\right)\right)$$

ET-Turb

Table 1. Parameter sampling ranges for ET-Turb dataset generation. Notation: $[a, b]$ denotes uniform sampling from continuous interval; $\{v_1, \ldots, v_n\}$ denotes uniform sampling from discrete set. All 12 configurations are sampled with equal probability.

Distance (m)	Focal length (m)	F-number	C_n^2 (10^{-14} m$^{-2/3}$)	Height (m)	Wind speed (m/s)	Exposure-time (ms)
[30,100]	[0.1,0.3]	{2.8,4}	[50,300]	{4,50}	[1,3]	[0.5,8]
		{2.8,4,5.6}	[200,500]	{100,200}	[3,5]	[0.5,8]
[100,200]	[0.2,0.5]	{2.8,4,5.6}	[5,50]	{200,400}	[1,4]	[1,20]
		{2.8,4,5.6,8}	[20,100]	{4,50}	[2,6]	[0.5,10]
[200,400]	[0.3,0.5]	{2.8,4,5.6,8}	[2,30]	{50,100}	[2,5]	[1,20]
		{4,5.6,8,11}	[10,40]	{10,50}	[3,6]	[1,20]
[400,600]	[0.4,0.75]	{4,5.6,8,11}	[1,20]	{50,150}	[3,5]	[2,40]
		{5.6,8,11,16}	[10,30]	{10,100}	[4,7]	[1,20]
[600,800]	[0.6,0.8]	{5.6,8,11,16}	[1,15]	{100,300}	[3,7]	[2,40]
		{8,11,16,18}	[2,20]	{50,200}	[4,8]	[2,40]
[800,1000]	[0.8,1]	{8,11,16,18}	[0.5,10]	{10,100}	[5,9]	[2,40]
		{11,16,18,24}	[1,20]	{4,50}	[6,10]	[1,20]

ET-Turb

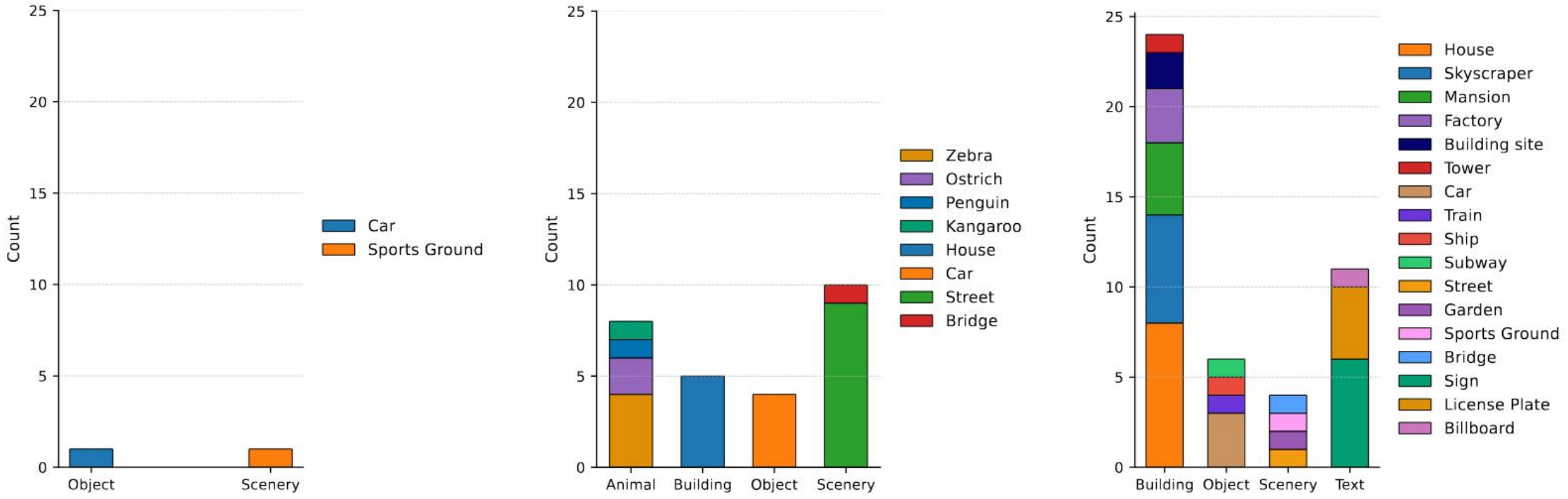

(a) Captured by Canon EOS-1D Mark IV [1]

(b) Captured by Nikon D750 [4]

(c) Captured by Nikon Coolpix P1000 [8]

Figure 1. ET-Turb-Real Dataset Composition: Multi-Camera Systems and Diverse Scene Distribution. Real-world turbulence data is collected across three different imaging devices, providing comprehensive coverage of diverse environmental and anthropogenic scenes: urban landscapes, entertainment venues, industrial infrastructure, traffic scenarios, and commercial establishments.

实验结果

Table 2. Quantitative comparison of turbulence mitigation models trained on different synthetic datasets and evaluated on real turbulence data. Models trained on ET-Turb dataset achieve consistently lower NIQE and BRISQUE scores (lower is better), confirming superior realism and generalization capability compared to TMT-Dynamic [50] dataset and ATSyn-Dynamic [49] dataset.

Training Dataset	TSR-WGAN [23]		TMT [50]		DATUM [49]		MambaTM [51]	
	NIQE ↓	BRISQUE ↓	NIQE ↓	BRISQUE ↓	NIQE ↓	BRISQUE ↓	NIQE ↓	BRISQUE ↓
TMT-dynamic [50]	4.231	52.502	4.361	58.581	4.219	54.921	4.217	55.062
ATSyn-dynamic [49]	4.224	54.462	4.483	59.707	4.308	59.126	4.247	56.876
ET-Turb	**4.190**	**50.981**	**4.221**	**56.691**	**4.204**	**54.070**	**4.212**	**55.050**

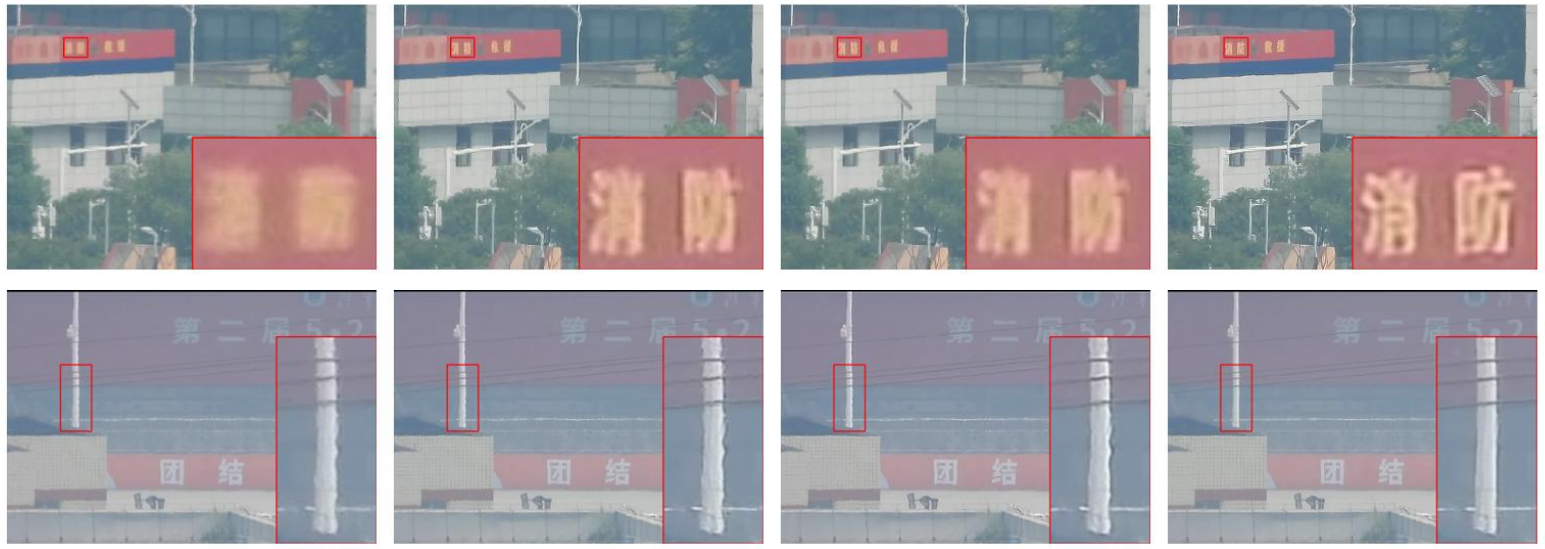

(a) Input (b) TMT-dynamic [50] (c) ATSyn-dynamic [49] (d) ET-Turb

Figure 5. Visual comparison of turbulence mitigation results on real data for MambaTM [51] models trained on different synthetic datasets. Models trained on ET-Turb dataset produce sharper and more natural restorations with fewer artifacts compared to those trained on TMT-Dynamic [50] dataset and ATSyn-Dynamic [49] dataset.

实验结果

Table 3. Ablation study on exposure modeling strategies within the ET-Turb synthesis pipeline. Comparing fixed ($\tau = 1$ms), binary ($\text{MTF}_{\text{SE/LE}}$), and continuous ($\text{MTF}_{\text{ET}}$) exposure formulations demonstrates that continuous modeling yields the best perceptual quality on MambaTM [51].

Exposure Strategy	NIQE ↓	BRISQUE ↓
ET-Turb ($\tau = 1$ms)	4.355	55.457
ET-Turb ($\text{MTF}_{\text{SE/LE}}$)	4.297	55.123
ET-Turb (MTF_{ET})	**4.212**	**55.050**

(a) Input (b) $\tau = 1$ms (c) $\text{MTF}_{\text{SE/LE}}$ (d) MTF_{ET}

Figure 6. Visual ablation study on exposure modeling strategies for real turbulence restoration. The continuous ET-MTF formulation produces more natural textures and stable structures compared to fixed or binary exposure approaches.

实验结果

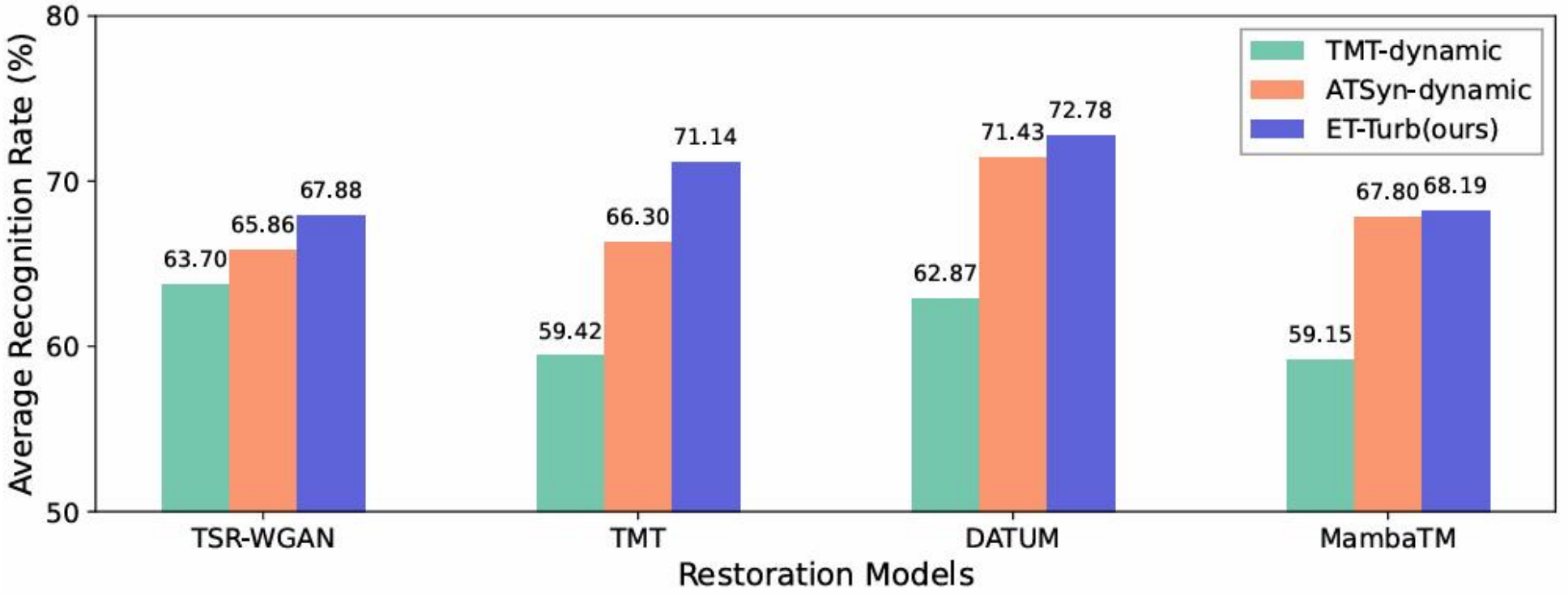

Figure 8. Text recognition accuracy on the turbulence-text dataset [54], evaluated using ASTER [44].